Passivation of Zinc Anodes in Alkaline Electrolyte: Part I. Determination of the Starting Point of Passive Film Formation

Marina Bockelmann,[1,2,z] Maik Becker,[1,2] Laurens Reining,[1,2] Ulrich Kunz,[1,2] and Thomas Turek[1,2]

[1] *Institute of Chemical and Electrochemical Process Engineering, Clausthal University of Technology, Clausthal-Zellerfeld 38678, Germany*
[2] *Forschungszentrum Energiespeichertechnologien, Goslar 38640, Germany*

In the present contribution we demonstrate a new testing cell, which allows simultaneous in situ optical and electrochemical investigations of passivation processes on zinc anodes in quiescent alkaline electrolytes. By combination of microscopy and galvanostatic impedance spectroscopy it was possible to detect the starting point of passive film formation, which has not been achieved so far. We found that formation of the so-called type 1 passive film is not dependent on the anodic current density. This passive film appears at electrode overpotentials of <0.15 V after an amount of zincate ions of approx. $8.2 \cdot 10^{-4}$ mol cm^{-2} has accumulated at the anode in a 30 wt% KOH electrolyte with 2 wt% ZnO at room temperature. Consequently, the passivation of zinc in quiescent electrolyte cannot be avoided even at very low dissolution currents. On the other hand, the so-called type 2 passive film appears below the first film due to direct oxidation of zinc. At overpotentials of ≥0.15 V the direct oxidation of zinc is favored and the potential-dependent type 2 passive film appears before type 1 film is formed.

 [DOI: 10.1149/2.0331813jes]

Manuscript submitted June 4, 2018; revised manuscript received August 30, 2018. Published September 25, 2018.

The increasing demand for large-scale stationary energy storage devices requires the development of new high-power and high-energy electrochemical systems. Among rechargeable metal-air batteries, zinc-air systems are considered as one of the most promising candidates due to several advantages of zinc as anode material. These include low equilibrium potential, relatively high stability in aqueous electrolytes, low equivalent weight, and high volumetric energy density. Furthermore, zinc is abundant, inexpensive and environmentally friendly. In the last decades major efforts have been made especially in the development of alkaline zinc-air systems.[1–3] However, electrically rechargeable alkaline zinc-air cells still suffer from low efficiency and insufficient cyclability, partially related to anodic passivation of the zinc electrode. Despite extensive earlier work published on the passivity of zinc in alkaline solutions[4] and several approaches to prevent the passive film formation,[2,5–9] no real breakthrough in this area could be achieved yet. Furthermore, there is little knowledge about the influence of operating conditions of a zinc-based battery on the passivation process and there are no well-tried in situ methods for the detection of passive films on working zinc electrodes.

Spectroscopic and microscopic investigations[10–13] of anodic zinc dissolution show that the passive film in its final state consists of zinc oxide. However, the films may appear in different modifications and colorations, depending on temperature as well as composition and flow conditions of the electrolyte.[14–17] Powers and Breiter[18] were the first who recognized the duplex nature of the film. These authors showed through microscopic observations during zinc passivation that in quiescent electrolyte a white and porous film (so-called type 1) appears first on the electrode surface while a denser film (type 2) appears beneath the first type later. Interestingly, the formation of type 1 passive film could be avoided in flowing electrolyte, but not that of type 2.[18] Thus, different causes and mechanisms of zinc passivation must exist, depending on the conditions of the electrochemical zinc dissolution.

Two principal mechanisms of passive film formation have been postulated: the "dissolution-precipitation" mechanism and the so-called "solid-state" reactions mechanism. Conforming to the "dissolution-precipitation" mechanism the zinc anode remains active until the concentration of zincate ions reaches a critical value and zinc salt precipitates onto the electrode surface. In contrast, passivation processes according to the "solid-state" reactions mechanism describes the direct oxidation of zinc due to anodic polarization.

One of the most important works on zinc passivation according to the "dissolution-precipitation" mechanism was published by Liu et al.[19] The results of these authors explain the formation of type 1 and type 2 passive films in quiescent conditions. According to them, the process of film formation can be divided into three steps. During step A the active zinc dissolution proceeds for a time t_{pass}, until the concentration of zincate ions in the vicinity of the electrode reaches the critical value (Fig. 1). From this time on the transport of zincate ions is disturbed and the type 1 passive film formation takes place during step B. Finally, the direct oxidation of zinc sets in due to a lack of hydroxide ions in the third passivation step C, during which type 2 passive film is supposed to form. If the remaining active electrode area is too small for the applied current density and sufficient driving

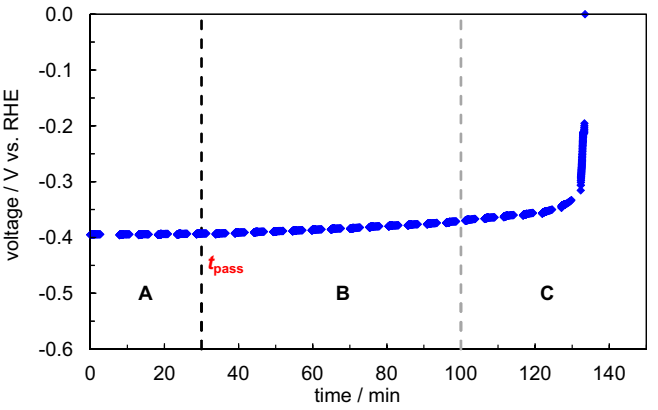

Figure 1. Potential curve of a zinc electrode during galvanostatic dissolution with 70 mA cm^{-2} at room temperature in 30 wt% KOH electrolyte with 2 wt% ZnO showing three passivation steps according to Liu et al.[19] During step A the active zinc dissolution proceeds for a time t_{pass}, until the concentration of zincate ions reaches the critical value. From this time on type 1 passive film forms during step B. Finally, the direct oxidation of zinc sets in in the third passivation step C, during which type 2 film forms. After the total passivation of the electrode the potential rises to that required for the oxygen evolution reaction.

[z] E-mail: marina.bockelmann@tu-clausthal.de

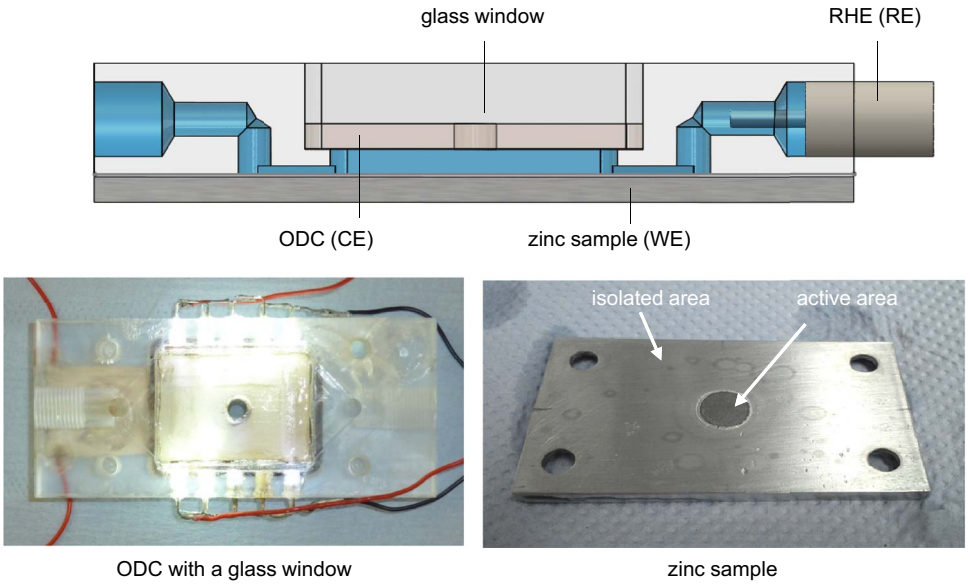

Figure 2. Measurement setup. The testing cell has total dimensions of 90 mm × 40 mm × 15 mm. The electrolyte volume is 10 ml. The active area of the zinc sample has a radius of 3 mm. The reference electrode has a distance of 30 mm to the active surface area of the zinc specimen.

potential is available, the potential of the electrode rises to that required for the oxygen evolution reaction.

In earlier work of other groups[20–22] the passivation time t_{pass} was determined from the potential jump at the end of the passivation process. For the operation of a zinc-based alkaline battery, it is, however, more important to examine the starting point of the passivation process and not its ending point. Liu et al.[19] interpreted instead the passivation time t_{pass} as the phase of active zinc dissolution until the onset of type 1 passive film formation (Fig. 1). Unfortunately, since the potential of the zinc anode increases homogeneously after applying a constant current and shows no abrupt changes (Fig. 1), it is not possible to determine the passivation time t_{pass} according to electrode potential.

The results of Liu et al. lead to the expectation that the critical zincate concentration would not be reached and thus the passivation could be completely avoided, as long as convection removes zincate ions from the electrode surface. However, especially potential controlled investigations show that a passive film is also formed in the presence of convection even after very short measurement times.[4] The onset of passivation during potential controlled measurement is supposed to proceed according to the "solid-state" reactions mechanism and is generally correlated with a sudden drop in current density to values of nearly zero. The active dissolution of zinc is presumed to occur up to a zinc overpotential of approx. 0.16 V.[23–26]

A closer look at the scientific literature on zinc passivation[4] reveals that the "dissolution-precipitation" mechanism was mainly used for the interpretation of galvanostatic measurements while the "solid-state" reactions mechanism was preferred in case of potentiodynamic investigations. Both mechanisms provide only a partial understanding of the complex passivation process and it can be overall summarized that no consensus about the underlying mechanism of zinc passivation has been reached yet.

Based on the considerations of Liu et al.,[19] the aim of our work was to provide an appropriate investigation method for measuring the passivation time t_{pass} during galvanostatic dissolution of zinc in quiescent alkaline electrolyte. Furthermore, we wanted to gain a better understanding of the complex passivation mechanism, which should explain experimental findings obtained both under galvanostatic and potentiodynamic conditions.

For this purpose we present a combination of microscopic and electrochemical impedance spectroscopy (EIS) measurements during anodic zinc dissolution at constant current density in quiescent electrolyte. Contrary to the potential controlled approach of Powers and Breiter[18] superimposed with optical observations, the constant current mode of our investigations leads to a gradual passivation of the zinc anode while in situ EIS and microscopic measurements provide additional information about the state of the electrode surface. With the help of these methods, we can successfully observe the starting point of type 1 film formation and also detect type 2 film formation without changing the experimental conditions. With these measurements and accompanying evaluations, based on a simple equivalent electrical circuit model, new insights into the mechanism of anodic zinc passivation could be obtained.

Experimental

Material.—The zinc specimens (purity 99.97 wt% with 0.015 wt% lead content, quality "K") with a thickness of 3 mm were provided by Grillo-Werke AG, Germany. The zinc samples were first polished with 320 and 800 grit fleece finishing pads and cleaned with acetone. Afterwards, the samples were sprayed with insulating varnish (Plastik 70, CRC Kontakt Chemie, Germany), excluding a circular active area with a radius of 3 mm, which was protected with electroplating tape (PortHole, Gamry Instruments, USA). Before the experiments the tape was removed from the electrode surface. As counter electrode an in-house produced silver-based oxygen depolarized cathode (ODC) was used, the preparation method and properties of which are described elsewhere.[27] The glass window in the ODC, required for the optical investigations, was bonded to the electrode with epoxy resin (Turbocoll 2000, Turbo Mix Universal, Bold & Co. OHG, Germany). All tests were performed in 30 wt% KOH electrolyte with 2 wt% ZnO at room temperature (RT), which is a suitable electrolyte composition for high-power zinc-air batteries.[28] The overpotentials of the zinc electrode were measured with a reversible hydrogen (RHE) reference electrode (mini-Hydroflex, Gaskatel, Germany).

Cell construction.—The testing cell made of acrylic glass allowed a horizontal arrangement of the electrodes, whereas the ODC with a glass window with a radius of 3 mm was placed on top and the zinc anode at the bottom (Fig. 2). The testing cell had total dimensions of 90 mm × 40 mm × 15 mm, while the gap between the electrodes was 7 mm and the electrolyte volume amounted to 10 ml. The ODC was operated with atmospheric oxygen in a self-breathing mode. To prevent any visual disruption by the formation of gas bubbles the cell was inclined by 15° (lengthwise). To enhance the visibility of the zinc

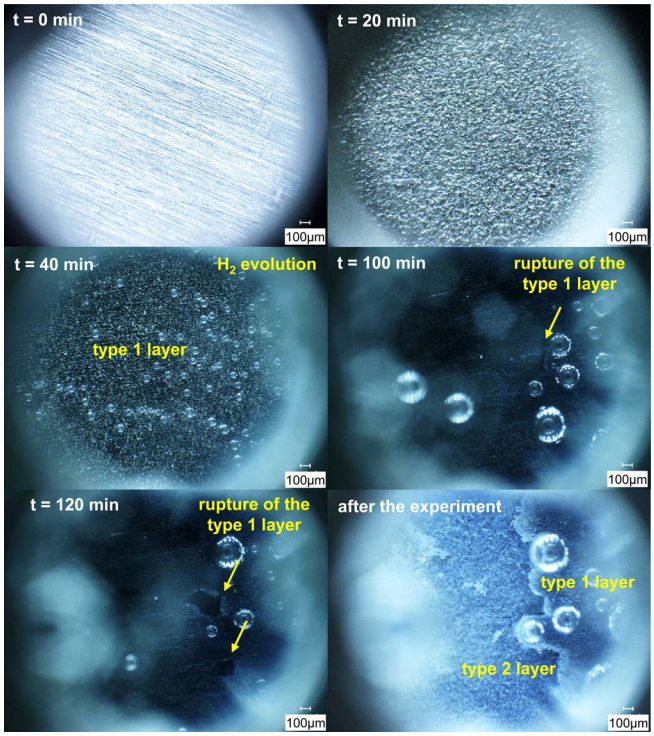

Figure 3. Microscopic in situ observations of zinc electrode surface during anodic passivation with constant current density of 70 mA cm^{-2}. The roughness of the electrode increases at the beginning of the dissolution. After 40 min the electrode loses the metallic gloss and formation of gas bubbles on the surface can be observed. During further dissolution of zinc a visible dark film appears above the electrode surface. After 100 min a rupture of this dark passive layer can be recognized. The measurement had to be finished after 130 min due to a determined potential jump caused by oxygen evolution. After the experiment two different passive layers can be identified on the surface of the zinc sample.

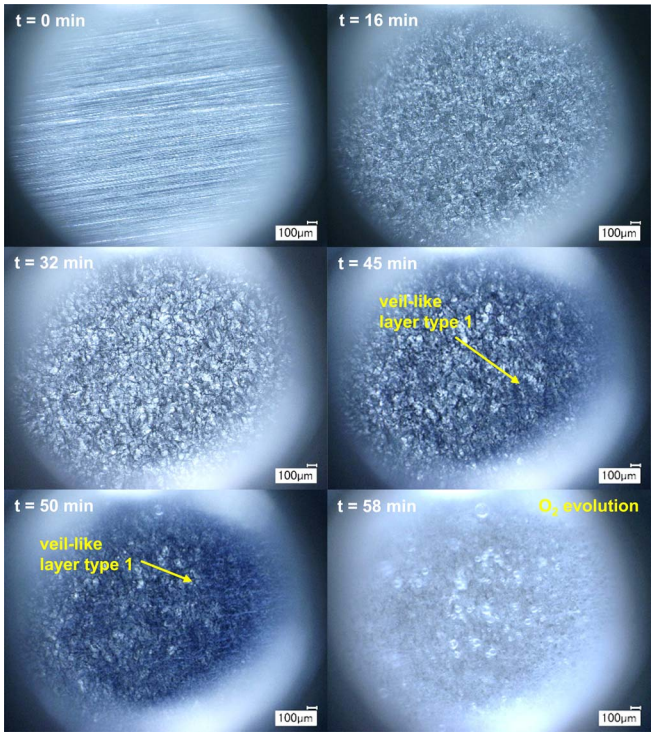

Figure 4. Microscopic in situ observations of zinc electrode surface during anodic passivation with constant current density of 110 mA cm^{-2}. The roughness of the electrode increases during the first minutes of dissolution. After 45 min type 1 passive film becomes visible on the right side of the sample, which covers nearly the whole electrode surface after further 5 min. The roughness of the electrode, however, remains visible. After 58 min of zinc dissolution the oxygen evolution reaction sets in, although the type 1 passive film has not yet become dense and coherent.

surface under the microscope ten small white LEDs with a light output of 22000 lm each (led-tech.de optoelectronics GmbH, Germany) were installed on the sides of the cell. The reference electrode was inserted into the cell from the lower inlet and had a distance of 30 mm to the active surface area of the zinc specimen.

Electrical and optical characterization.—The passivation of zinc samples was characterized in quiescent electrolyte using a Gamry Reference 3000 potentiostat and a Keyence VHS-2000D microscope. For each experiment a fresh zinc electrode was conditioned and placed into the measurement setup. After filling the cell with KOH solution the experiment was immediately started. During anodic polarization of zinc with constant current galvanostatic electrochemical impedance spectra (EIS) with the same DC current were recorded every 180 s. For reasons of signal quality the EIS measurements were divided into two frequency ranges: from 100 000 Hz to 100 Hz with applied AC current of 1 mA rms and from 100 Hz to 0.1 Hz with applied AC current of 0.5 mA rms. After each impedance measurement a microscopic picture of the electrode surface was taken. The experiment was finished after the potential jump, related to the oxygen evolution at passivated zinc surface as described above (Fig. 1).

Results and Discussion

Microscopic observations.—In Fig. 3 exemplary in situ observations of the electrode surface during the passivation process at 70 mA cm^{-2} are presented. The microscopic pictures show that the roughness of the electrode increases at least during the first 20 min of dissolution. After 40 min the electrode loses the metallic gloss and formation of gas bubbles on the surface can be observed. Given the negative potential of zinc the gas bubbles are presumed to be hydrogen. In previous studies Farmer and Webb[22] as well as Sanghi and Fleischmann[29] also proposed the formation of hydrogen. These authors assumed that the zinc oxide film could act as a hydrogen evolution catalyst. It could, however, be that hydrogen is already formed on the active electrode surface because of the natural zinc dissolution due to the negative standard electrode potential of zinc in alkaline media, but that these bubbles are too tiny to be visible under the microscope, probably because of electrochemical reduction (Fig. 3, t <40 min). The arising passive layer could prevent the electrode from further natural dissolution and on the other hand promote the growth of hydrogen bubbles.

During further dissolution of zinc a visible dark film appears above the electrode surface so that the roughness of the electrode can no longer be identified. After 100 min a rupture of this dark passive layer can be recognized, which becomes more significant during further polarization of the electrode. Despite the cracks in the passive layer and a corresponding expected rise of the electrode activity the measurement had to be finished after 130 min due to an observed potential jump caused by oxygen evolution (Fig. 1). After the experiment two different passive layers could be identified on the surface of the zinc sample, which confirms the observations of Powers and Breiter[18] and Lui et al.[19] The distance between the type 1 and type 2 passive films was microscopically determined to be of the order of 200 µm.

Microscopic observations in Fig. 4 show that the passivation process at 110 mA cm^{-2} is different from that at lower current densities (cf. Fig. 3). Similar to experiments at current density of 70 mA cm^{-2}, the roughness of the electrode increases at 110 mA cm^{-2} during the first minutes of dissolution. However, no formation of hydrogen bubbles on the zinc surface can be observed. After 45 min type 1 passive film becomes visible on the right side of the sample (lower electrolyte

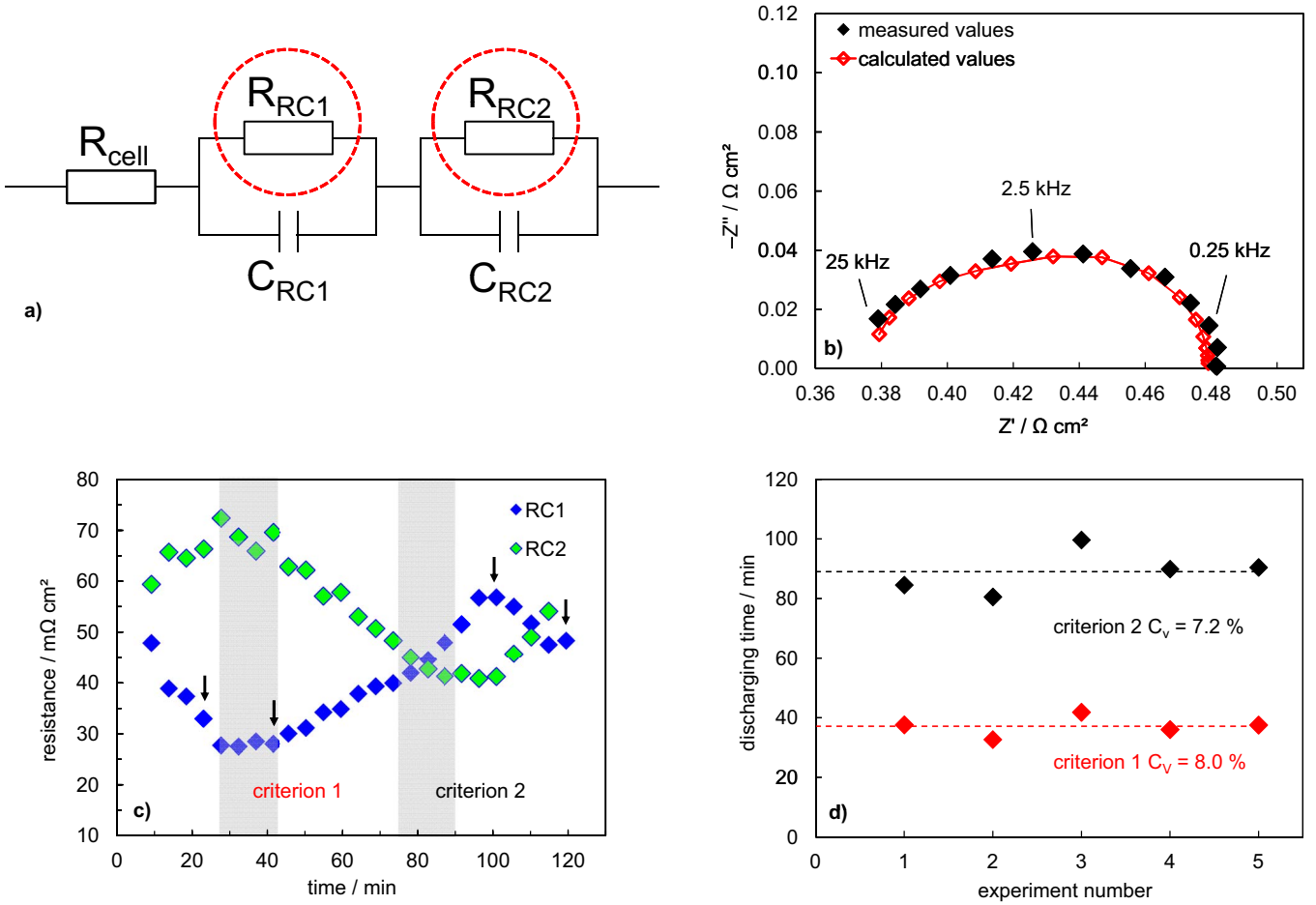

Figure 5. EIS investigations of the zinc electrode kinetics during anodic polarization at constant current density of 70 mA cm^{-2}: (a) equivalent electrical circuit model for anodic zinc dissolution. R_{cell} represents the ohmic cell resistance, R_{RC1} the kinetic resistance of the reaction from Zn to Zn^{I} (I), R_{RC2} the kinetic resistance of the reaction Zn^{I} to Zn^{II} (II), C_{RC1} and C_{RC2} the related double layer capacities; (b) example of measured and calculated EIS spectra from 30 000 Hz to 20 Hz according to the equivalent electrical circuit model in (a). EIS spectra were measured in the galvanostatic mode with the same DC current as during the anodic polarization; (c) trends of R_{RC1} and R_{RC2} as a function of dissolution time. Criterion 1 area corresponds to the minimum value of the resistance R_{RC1} and identifies the beginning of the type 1 film formation. The time at which both ohmic resistances R_{RC1} and R_{RC2} reach equivalent values was chosen as criterion 2. Small arrows mark points corresponding to the microscopic images in Fig. 3; (d) reproducibility and coefficients of variation for criterion 1 and criterion 2, defined in (c).

level due to the inclination of the cell). During further 5 min a loose and flocculent type 1 passive film covers nearly the whole electrode surface, but the roughness of the electrode remains visible. After 58 min of zinc dissolution with 110 mA cm^{-2}, the oxygen evolution reaction sets in, although the type 1 passive film has not yet become dense and coherent like in passivation experiments at lower current densities (Fig. 3).

EIS investigations and development of an equivalent electrical circuit model.—Independently of the state of the electrode – whether active or passive – and of the specific reaction path with corresponding reaction products, zinc oxidizes in two electron transfer steps from Zn to Zn^{I} and finally to Zn^{II}, whereby the second step is rate-determining (rds.):[30,31]

$$Zn \leftrightarrows Zn^{I} + e^{-} \qquad [I]$$

$$Zn^{I} \leftrightarrows Zn^{II} + e^{-} \quad rds. \qquad [II]$$

Exemplary results of the described EIS measurements are shown in Fig. 5b and Fig. S1. The spectrum consists of two semicircles, referring to two electron transfer Reactions I and II. Thus, the impedance spectroscopic data can be described with an equivalent electrical circuit model (EECM) consisting of two RC networks (Fig. 5a), which is widely used for passivation studies of electrode surfaces.[32–34] In this work solely the ohmic components of the RC networks R_{RC1} and R_{RC2} are of interest.

The model describes the measured values of the impedance spectrum (Fig. 5b) sufficiently well, thus a calculation of the ohmic resistances R_{RC1} and R_{RC2} is possible. We want to point out once more that EIS spectra were measured in the galvanostatic mode with the same DC current as during the anodic polarization of zinc with constant current densities of up to 110 mA cm^{-2}. Considering the impaired quality of the EIS spectra, the ambition of a more accurate fit of the measured data is not reasonable. In order to calculate the kinetic parameters of anodic zinc reactions more precisely, EIS measurements at the quasi-steady-state conditions are required. This is, however, not the focus of this work.

In Fig. 5c the development of R_{RC1} and R_{RC2} is presented as a function of time. Due to the galvanostatic mode of EIS measurements the adjusted current is splitted between electron transfer reactions according to their kinetics. Therefore, R_{RC1} and R_{RC2} are anticorrelated parameters and depend on each other. To understand the development of R_{RC1} and R_{RC2}, a conjunction with the microscopic results (Fig. 3) is required.

Interpretation of combined microscopic and EIS results.—At the beginning of the experiment in Fig. 5c the resistance R_{RC1} decreases, while R_{RC2} grows. Microscopic investigation shows that the roughness

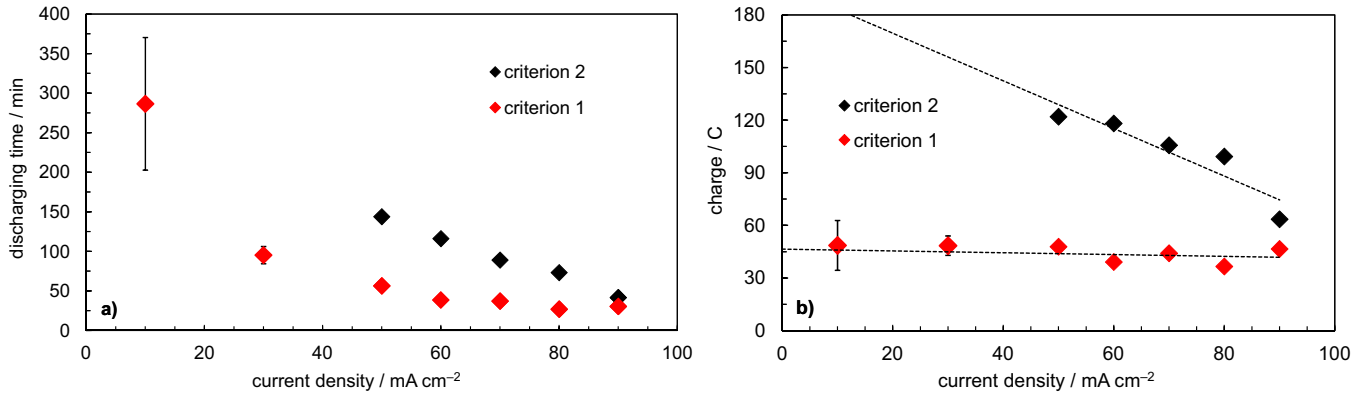

Figure 6. Influence of dissolution current density on passivation criterions 1 (red) and 2 (black), as defined in Fig. 5c: (a) discharging time and (b) transferred electrical charge as a function of current density.

of the zinc specimen increases at this stage. Higher roughness leads to larger surface area and eventually to a reduced kinetic resistance R_{RC1}. After 30 minutes R_{RC1} reaches a minimum and begins to increase again. At the same time the microscopic images show that the electrode loses its metallic gloss and hydrogen bubbles on the zinc surface become visible.

The increasing electrode surface affects the kinetics of the reaction step (I) positively, which correlates with decreasing values of R_{RC1}. From the moment at which the electrode loses its metallic gloss, appears darker and growing H_2 bubbles can be recognized, a passive film forms on the electrode. This film prevents the zinc electrode from further oxidation according to Reaction I. The fact that the ohmic resistance R_{RC1} reaches its minimum value and starts to increase with the formation of the passive film can be explained with the assumption that R_{RC1} describes the kinetics of the first reaction step of zinc dissolution (I). It is therefore important to investigate the influence of operating parameters on the minimum value of the resistance R_{RC1}, marked as criterion 1 area in Fig. 5c, which identifies the beginning of the type 1 film formation. Consequently, the ohmic resistance R_{RC2} describes the second step of the zinc oxidation Reaction II and expresses the kinetics of the zinc oxide formation after passing the criterion 1. Microscopic observations support this assumption (Fig. 3, 100 min). After a duration of 100 min a rupture of the passive layer can be recognized, which becomes more significant during further polarization of the electrode. Increasing electrode activity and improved transport of hydroxide ions due to the damage of the passive layer reduces the value of R_{RC1} and raise R_{RC2} (Fig. 5c).

The time at which both ohmic resistances R_{RC1} and R_{RC2} reach equivalent values was chosen as criterion 2 for further investigations of the zinc passivation process (Fig. 5c). From this moment on, the kinetics of the reaction of Zn to Zn^{I} become slower than those of the subsequent reaction of Zn^{I} to Zn^{II}. After the formation of both passive films the EIS signal becomes unstable and invalid. Therefore Fig. 5c does not show kinetic resistances referring to the stage of oxygen evolution.

The trends for R_{RC1} and R_{RC2} were mathematically described with third-order polynomials, so that the minimum for R_{RC1} and the intersection between R_{RC1} and R_{RC2} could be precisely calculated. The reproducibility of the results was closely examined for a current density of 70 mA cm^{-2}. In Fig. 5d coefficients of variation (C_V) for criterion 1 and criterion 2 from five different measurements are shown. Both coefficients of variation are lower than 10%, which is an accurate result for investigations of zinc passivation.[4]

As presumed by Liu et al.,[19] type 1 passive film would form after the concentration of zincate ions in the vicinity of the electrode exceeds a critical value. According to this suggestion, the times for reaching the passivation criterions 1 and 2 (Fig. 5c) should depend on the anodic current density. At lower currents the formation rate of zincates is also lower and, due to the movement of zincates from the zinc electrode surface into the bulk solution, the passivation time should increase. Furthermore, the depletion of hydroxide ions near the electrode is also diminished at lower currents, prolonging the process of the active zinc dissolution. Fig. 6a shows the influence of different current densities on the discharging time until the passivation criterions are reached. Red diamonds describe results of the first passivation criterion. Measurements at dissolution currents of 50–90 mA cm^{-2} show good reproducibility so that the error bars are not visible behind the symbols of measurement points. However, due to the slope of the testing cell of 15°, the natural convection contributes to the transport of zincates from the electrode which becomes evident at lower current densities and accordingly long passivation times. This results in increasing degree of variation and higher error bars for 10–30 mA cm^{-2} in Fig. 6. Black diamonds describe results of passivation criterion 2. The discharging time until type 2 passive film appears shows a stronger dependence on the current density than for type 1 film. According to the "solid-state" reactions mechanism the formed film is non-uniform and consists of discrete nuclei, which may be two-dimensional or three-dimensional in nature. During the passivation process these nuclei coalesce and form a continuous film with varying thickness. At higher dissolution currents the non-uniformity and the thickness of the layer increase and therefore lead to reduced passivation times.[35,36]

For a better comparability and understanding it is more useful to regard the influence of the current density on the transferred electrical charge, which corresponds to the amount of formed zincate ions (Fig. 6b). A very surprising finding provide the results of passivation criterion 1. The formation of the passive film type 1 seems to be hardly affected by the dissolution rate of the electrode. On the other hand, the very low slope of the linear trend in Fig. 6b reveals that the amount of transferred electric charge and thus formed zincate ions, at which the passivation criterion is reached, is nearly constant for different current densities. It could be concluded that zincate ions rather accumulate at the electrode surface than move into the bulk solution. One possible reason for this effect could be the polymerization of zincate ions in the supersaturated region near the electrode due to a lack of water molecules and hydroxide ions, as it was stated by Dirkse.[37] Our microscopic observations (Video S2) confirm the suggestions of Dirkse and clearly show the formation of a coherent dark passive layer in a certain distance from the electrode. Other groups described similar findings.[36,38–40] Furthermore, at the surface of zinc anodes a 30% higher zinc ion concentration was found than in the bulk solution by Eisenberg et al.[41] for ZnO saturated 30 wt% KOH solution.

Using Einsteins diffusion equation, it is possible to calculate the time which zincate ions would need to diffuse through the testing cell (Fig. 2):

$$D_{Zn(OH)_4^{2-}} = \frac{{x_{cell}}^2}{2\, t_{diff}} \qquad [1]$$

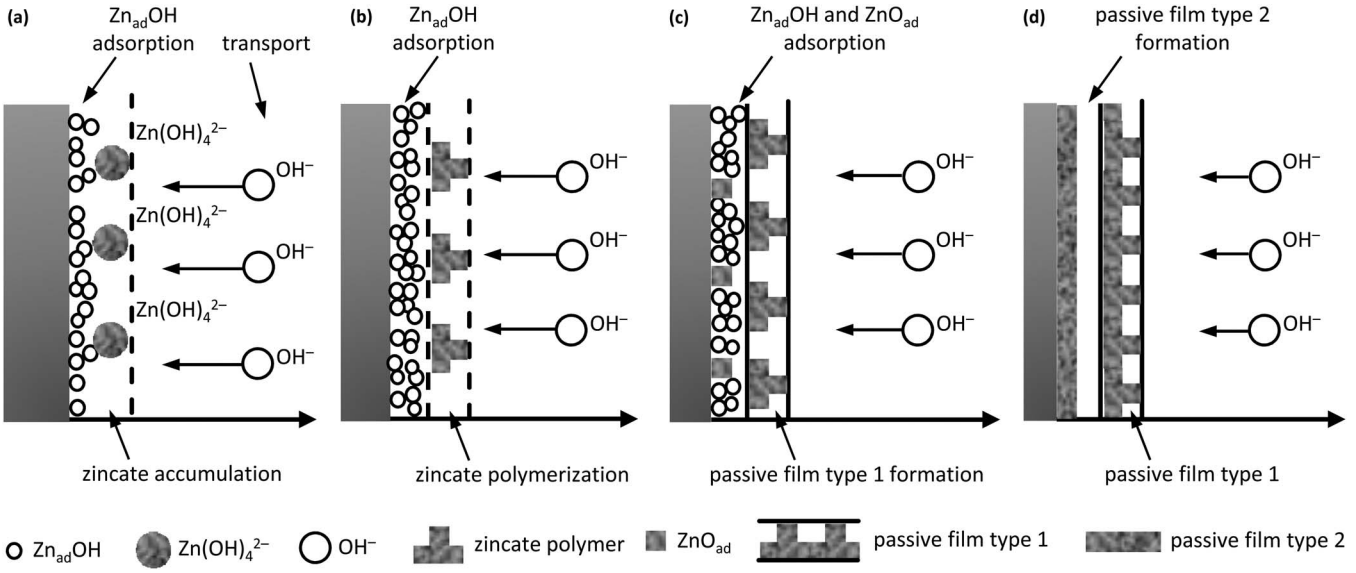

Figure 7. Schematic representation of the development of anodic passive films on zinc: (a) active zinc dissolution; (b) formation of polymerization region where zincate intermediates polymerize and form a coherent passive layer; (c) formation of type 1 passive film, which hampers diffusion of zincates and increases ionic resistance; (d) nucleation and growth region of type 2 passive film, that leads to its complete passivation.

With the diffusion coefficient $D_{Zn(OH)_4^{2-}}$ of zincate ions[42,43] of approx. $2.0 \cdot 10^{-6}$ cm^2 s^{-1} and the cell thickness x_{cell} of 7 mm, the diffusion time t_{diff} of zincate ions reaches a value of 34 hours. The time the type 1 passive film needs to form is in the range of 0.5 hours (Fig. 5b). Therefore, it is highly likely that zincate ions rather form a stable network in the vicinity of the electrode instead of diffusing into the bulk solution, which would explain the nearly constant charge value for reaching criterion 1 despite different dissolution rates. According to this assumption, Fig. 7 represents a possible mechanism of zinc passivation. During the active zinc dissolution zincate ions remain near the surface of the zinc electrode (Fig. 7a). Because of their rising concentration zincate intermediates polymerize and form a coherent passive layer (Fig. 7b). The further dissolution of the electrode leads to its continuous removal and to the growth of the gap between the electrode surface and the passive layer. The porous structure of the type 1 passive layer still allows the transport of hydroxide ions to the electrode but hampers the diffusion of zincates. Thickness and density of the passive layer increase and therefore its ionic resistance grows. First ZnO adsorbs at the electrode surface (Fig. 7c). Finally, the formation of a coherent type 2 passive film prevents the electrode from further dissolution and leads to its complete passivation (Fig. 7d). However, the question remains what the exact cause for the formation of type 2 passive film is. The thickening of the type 1 passive film could provoke the depletion of hydroxide ions and hamper further dissolution of the electrode according to Reaction I. As a result of the galvanostatic mode during the experiments, the potential of the electrode shifts to more positive values. Thus, the resulting overpotential could lead to the direct oxidation of the zinc surface (Fig. 7c). A comparison of the zinc electrode overpotentials during the active dissolution with overpotentials at those points where the two passivation criterions are met provides insight into this issue (Fig. 8a).

The electrode overpotentials η_1 at passivation criterion 1 are very similar to the values η_i at non-passivated electrodes for current densities of 30–90 mA cm^{-2}. The electrode overpotentials η_2 at passivation criterion 2 differ more clearly from that of active zinc and vary slightly between 0.12 V and 0.14 V. It is therefore apparent that the passivation criterion 2 and consequently the formation of type 2 passive film are, in contrast to type 1, primarily dependent on the overpotential at the zinc electrode. In order to prove our assumption, we increased the dissolution current density of zinc to 110 mA cm^{-2} to immediately reach

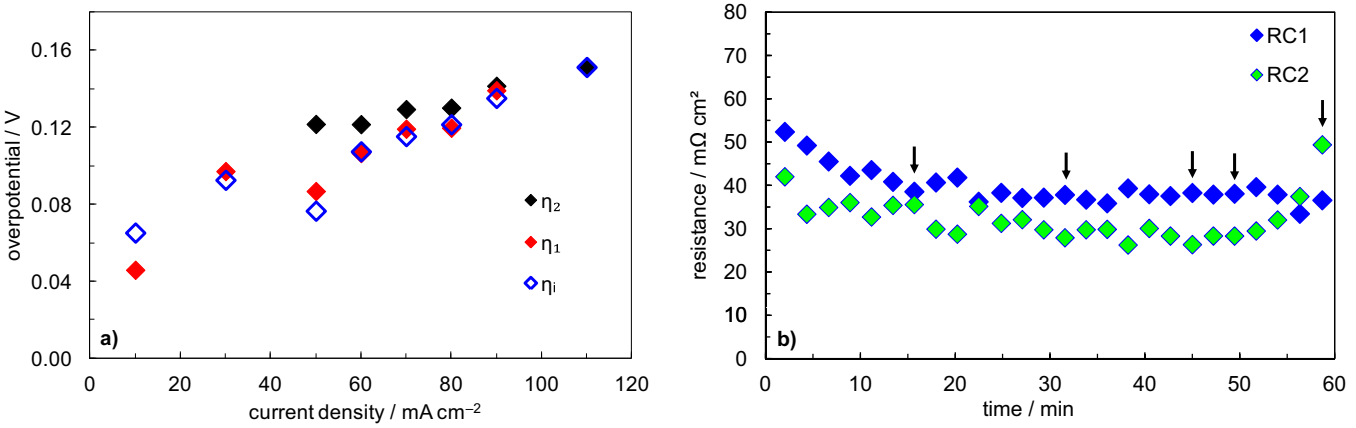

Figure 8. Influence of the zinc anode overpotential on the passivation process: (a) zinc electrode overpotentials during galvanostatic dissolution of non-passivated zinc (η_i), at passivation criterion 1 (η_1) and at passivation criterion 2 (η_2); (b) kinetic resistances R_{RC1} and R_{RC2} of zinc dissolution reaction at constant current density of 110 mA cm^{-2} as a function of dissolution time. Small arrows mark points corresponding to the microscopic images in Fig. 4.

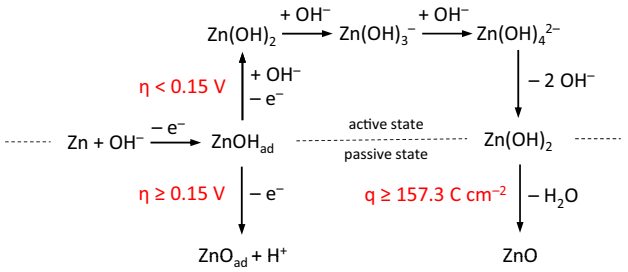

Scheme 1.

an anodic electrode overpotential of 0.15 V. In contrast to the results shown in Fig. 5c for 70 mA cm^{-2}, R_{RC1} is already at the beginning of the measurements higher than R_{RC2} (Fig. 8b). It can thus be concluded that electrode overpotentials from 0.15 V on promote the direct oxidation of the electrode according to the "solid-state" reactions mechanism and the type 2 passive film appears at the electrode surface before the type 1 passive film is formed. This result complies with previous findings of other groups who specified an anodic zinc overpotential of 0.16 V as the limiting value of the active zinc dissolution reaction.[23–26] Microscopic observations in Fig. 4 additionally confirm our conclusions. As previously described, the oxygen evolution reaction sets in before the type 1 passive layer fully covers the electrode surface. The type 2 passive layer must therefore have formed beneath the layer type 1. It is therefore unequivocal that from anodic zinc overpotentials of ca. 0.15 V, the main passivation process changes from the zincate amount dependent "dissolution-precipitation" mechanism to the electrode potential dependent "solid-state" reactions mechanism. The formation of type 1 passive film can still be observed, the direct oxidation of zinc, however, becomes the faster and more dominant reaction. According to our findings, the overall mechanism of zinc oxidation in alkaline electrolyte can be described due to Scheme 1.

The results depicted in Fig. 6 show that the formation of the type 1 passive film in quiescent electrolyte also takes place at very low dissolution current densities. Furthermore, the amount of zincate ions, at which the passivation criterion 1 is reached, is almost independent of the dissolution rate. According to the mean value of transferred charge of 44.47 C (cf. Fig. 6b, red diamonds), the required electrical charge density for the onset of passive film type 1 formation is approx. 157.3 C cm^{-2}, which corresponds to $8.2 \cdot 10^{-4}$ mol cm^{-2} zincate ions. Using this finding it is possible to predict the maximum discharging time of a zinc electrode at current densities lower than the chosen measuring range of 10–90 mA cm^{-2}. Red diamonds in Fig. 9 correspond to results of the first passivation criterion (cf. Fig. 6a). Blue diamonds demonstrate the predicted values, calculated on the basis of

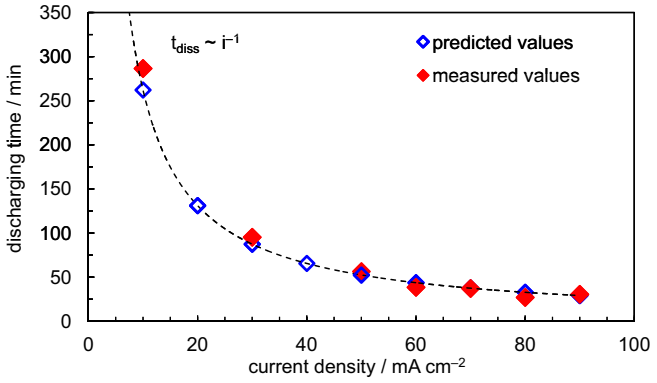

Figure 9. Measured and calculated discharging times until formation of type 1 passive film starts. Red diamonds correspond to results of the first passivation criterion (cf. Fig. 6a). Blue diamonds demonstrate the predicted values, calculated on the basis of constant electrical charge of 157.3 C cm^{-2}.

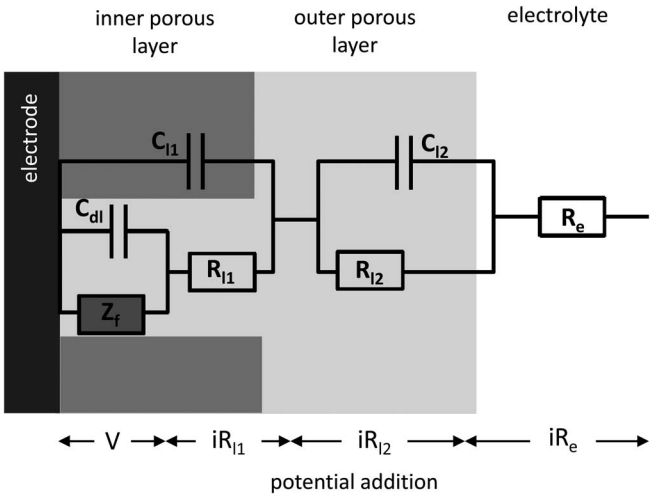

Figure 10. Equivalent electrical circuit of the impedance for an electrode coated by two superimposed porous layers (after Orazem and Tribollet).[45] It considers, that both passive layers are not insulators, that the electrolyte resistance within the pore differs from the resistance of the bulk electrolyte, and that a mass-transport resistance exists.

constant electrical charge of 157.3 C cm^{-2}. The discharging time of a zinc electrode is thus a function of the reciprocal value of the current density. Consequently, the formation of the passive film type 1 cannot be avoided even at very low dissolution rates in alkaline electrolyte without convection.

The presented in situ investigations of zinc passivation show the complexity of this process. The applied simplified equivalent electrical circuit model (Fig. 5a) was previously used to describe electrochemical oxidation reactions of metal-based electrodes by other groups[32–34,44] and provided good results in our work on zinc oxidation. However, for an exact description of the electrochemical reactions occurring during zinc passivation in alkaline solution, a more detailed EECM would be required. Furthermore, since the zinc electrode undergoes considerable changes during the experiments (transition from active to passive state), the EECM should be adapted in accordance with these changes. Therefore, knowledge of the exact time, at which the surface of the zinc anode and the passive film modify, is necessary. In view of the amount of measurement data, the main aim of our work was to develop a simple and quickly evaluable model which would be able to display this passive film modifications in accordance with the microscopic observations shown in Fig. 3 and Fig. 4. Given the good agreement between microscopic and EIS results, our work can be regarded as successful and the simplified EECM (Fig. 5a) as a good starting point for further model developments.

A suitable EECM for more detailed description of the zinc passivation could be the model of Orazem and Tribollet,[45] which describes the impedance of an electrode coated by two superimposed porous layers (Fig. 10). It takes into account that both passive layers are not insulators, that the electrolyte resistance within the pore differs from the resistance of the bulk electrolyte, and that a mass-transport resistance exists. Other possible EECMs were also proposed.[46–49] With the knowledge from our work, the progress of the passivation process on zinc anodes can be specifically adjusted, allowing subsequent determination of physical parameters of the passive layers with a more detailed EECM in future work.

Conclusions

In the present contribution we describe a new experimental approach for determination of the passive film formation on zinc anodes in quiescent alkaline electrolyte. The developed testing cell allows the simultaneous performance of in situ optical and electrochemical investigations during passivation. The combination of these methods

enables the determination of the passivation time which corresponds to the starting point of the passivation process. With the help of optical microscopy, we observed the appearance of two different passive films (type 1 and type 2) and defined suitable criteria from EIS measurements with which the onset of particular passive film formation can be identified. Furthermore, we determined that type 1 passive film arises after an amount of zincate ions of $8.2 \cdot 10^{-4}$ mol cm^{-2} accumulates in the vicinity of the electrode, while the formation of type 2 passive film starts once an overpotential at the electrode of ca. 0.15 V is reached. In our galvanostatic experiments we could observe the formation of passive films not only according to the "dissolution-precipitation" model, as expected, but also according to the "solid-state" reactions mechanism, which has not yet been demonstrated by other groups. Consequently, we could derive a coherent idea of the overall mechanism of zinc passivation in alkaline media, regardless of specific experimental conditions or measuring techniques.

Acknowledgment

Parts of this work was supported by the German Federal Ministry for Economic Affairs and Energy (grant number 03ESP217 E) during the ZnPLUS project. The authors furthermore thank Bernard Tribollet from the Laboratory of Interfaces and Electrochemical Systems at Pierre and Marie Curie University, Paris, Hansjörg Lehmkuhl from the Bauhaus-Universität Weimar and Karin Bode from the Institute of Inorganic and Analytical Chemistry at Clausthal University of Technology, for helpful discussions, as well as Petra Gehrke from Grillo-Werke AG, for providing the zinc samples.

ORCID

Marina Bockelmann https://orcid.org/0000-0003-1593-0051
Thomas Turek https://orcid.org/0000-0002-7415-1966

References

1. K. Harting, U. Kunz, and T. Turek, *Z. Phys. Chem.*, **226**(2), 151 (2012).
2. A. R. Mainar, O. Leonet, M. Bengoechea, I. Boyano, I. de Meatza, A. Kvasha, A. Guerfi, and J. Alberto Blázquez, *Int. J. Energy Res.*, (2016).
3. G. X. Zhang, *ECS Trans.*, **16**(34), 47 (2009).
4. M. Bockelmann, L. Reining, U. Kunz, and T. Turek, *Electrochim. Acta*, **237**, 276 (2017).
5. D. Stock, S. Dongmo, K. Miyazaki, T. Abe, J. Janek, and D. Schröder, *J. Power Sources*, **395**, 195 (2018).
6. M. Schmid and M. Willert-Porada, *Electrochim. Acta*, **260**, 246 (2018).
7. K. Liu, P. He, H. Bai, J. Chen, F. Dong, S. Wang, M. He, and S. Yuan, *Mater. Chem. Phys.*, **199**, 73 (2017).
8. Z. Zhou, Y. Zhang, P. Chen, Y. Wu, H. Yang, H. Ding, Y. Zhang, Z. Wang, X. Du, and N. Liu, *Chem. Eng. Sci.*, (2018).
9. G. Prentice, Y. C. Chang, and X. Shan, *J. Electrochem. Soc.*, **138**(4), 890 (1991).
10. W.-B. Cai, Q. Shi, M. F. Mansuetto, and D. A. Scherson, *Electrochem. Solid-State Lett.*, **3**(7), 319 (2000).
11. C. G. Smith, *Ellipsometry of anodic film growth*, University of California, Berkeley, California (1978).
12. A. Hugot-Le Goff, S. Joiret, B. Saïdani, and R. Wiart, *J. Electroanal. Chem. Interfacial Electrochem.*, **263**(1), 127 (1989).
13. Q. Shi, L. J. Rendek, W.-B. Cai, and D. A. Scherson, *Electrochem. Solid-State Lett.*, **6**(11), E35 (2003).
14. Z. I. Nikitina, *J. Appl. Chem. USSR*, **31**(209), 209 (1958).
15. K. Huber, *Helv. Chim. Acta*, **26**(4), 1037 (1943).
16. K. Huber, *J. Electrochem. Soc.*, **100**(8), 376 (1953).
17. R. D. Armstrong and M. F. Bell, in *Electrochemistry*, H. R. Thirsk, ed., Vol. **4**, p. 1, The Royal Society of Chemistry, (1974).
18. R. W. Powers and M. W. Breiter, *J. Electrochem. Soc.*, **116**(6), 719 (1969).
19. M. B. Liu, G. M. Cook, and N. P. Yao, *J. Electrochem. Soc.*, **128**(8), 1663 (1981).
20. N. A. Hampson, M. J. Tarbox, J. T. Lilley, and P. G. Farr, *Electrochem. Technol.*, **2**(11–12), 309 (1964).
21. T. P. Dirkse and D. J. Kroon, *J. Appl. Electrochem.*, **1**, (1971).
22. E. D. Farmer and A. H. Webb, *J. Appl. Electrochem.*, **2**(2), 123 (1972).
23. M. N. Hull, J. E. Ellison, and J. E. Toni, *J. Electrochem. Soc.*, (1970).
24. M. N. Hull and J. E. Toni, *T. Faraday Soc.*, **67**(0), 1128 (1971).
25. P. L. Cabot, M. Cortes, C. F., and E. Perez, *J. Appl. Electrochem.*, **23**, 371 (1992).
26. T. P. Dirkse and N. A. Hampson, *Electrochim. Acta*, **17**(3), 387 (1972).
27. I. Moussallem, S. Pinnow, N. Wagner, and T. Turek, *Chem. Eng. Process.*, **52**, 125 (2012).
28. M. Bockelmann, U. Kunz, and T. Turek, *Electrochem. Commun.*, **69**, 24 (2016).
29. I. Sanghi and M. Fleischmann, *Electrochim. Acta*, **1**, 161 (1959).
30. C. Cachet, B. Saidani, and R. Wiart, *J. Electrochem. Soc.*, **138**(3), 678 (1992).
31. C. Cachet, B. Saidani, and R. Wiart, *J. Electrochem. Soc.*, **139**(3), 645 (1992).
32. L. Brinkhaus, *Degradation phenomena of lithium-rich lithium-nickel-cobalt-manganese-oxide in lithium-ion-batteries*, Friedrich-Alexander-Universität Erlangen-Nürnberg (FAU) (2015).
33. A. Fattah-Alhosseini, S. Taheri Shoja, B. Heydari Zebardast, and P. Mohamadian Samim, *Int. J. Electrochem.*, 2011, 1 (2011).
34. M. Szklarska, G. Dercz, W. Simka, and B. Łosiewicz, *Surf. Interface Anal.*, **46**(10–11), 698 (2014).
35. A. J. Bard, *Encyclopedia of electrochemistry of the elements*, Marcel Dekker INC., New York, Basel (1976).
36. R. D. Armstrong, *Corros. Sci.*, **11**(10), 693 (1971).
37. T. P. Dirkse, *J. Electrochem. Soc.*, **128**(7), 1412 (1981).
38. S. Thomas, N. Birbilis, M. S. Venkatraman, and I. S. Cole, *Corros. Sci.*, **69**, 11 (2013).
39. A. G. Briggs, N. A. Hampson, and A. Marshall, *J. Chem. Soc., Faraday Trans. 2*, **70**(0), 1978 (1974).
40. C. Debiemme-Chouvy and J. Vedel, *J. Electrochem. Soc.*, **138**(9), 2538 (1991).
41. M. Eisenberg, H. F. Bauman, and D. M. Brettner, *J. Electrochem. Soc.*, **108**, 909 (1961).
42. E. Deiss, F. Holzer, and O. Haas, *Electrochim. Acta*, **47**(25), 3995 (2002).
43. E. J. Pessine, S. M. L. Agostinho, and H. C. Chagas, *Can. J. Chem.*, **64**, 523 (1984).
44. A.-R. El-Sayed, H. S. Mohran, and H. M. Abd El-Lateef, *Metall. Mater. Trans. A*, **43**(2), 619 (2012).
45. M. E. Orazem and B. Tribollet, in *Electrochemical impedance spectroscopy*, p. 153, John Wiley & Sons, Inc., (2008).
46. A. Fattah-Alhosseini and N. Attarzadeh, *Int. J. Electrochem.*, **2011**, 1 (2011).
47. L. Sziráki, Á. Cziráki, I. Geröcs, Z. Vértesy, and L. Kiss, *Electrochim. Acta*, **43**(1–2), 175 (1998).
48. M. Metikoš-Huković and Z. Grubač, *J. Electroanal. Chem.*, **556**(0), 167 (2003).
49. G. Vázquez and I. González, *Electrochim. Acta*, **52**(24), 6771 (2007).